



or decays in the presence of magnetic damping – to a spatially homogeneous state.

Magnetic soliton topology yields important information about the collective behavior of multiple solitons. For example, domain walls with opposite chirality can annihilate into a



PMA [5]. The topological bion stripe is of particular interest because its structure is reminiscent of chiral Néel domain walls [40,41] that have been recently utilized to nucleate skyrmions [24,35,36]. In the following, we will refer to nontopological or topological bion stripes according to their one-dimensional chirality.

### III. BION FILAMENT STABILITY ANALYSIS

To study the stability of bion stripes, we determine the evolution of perturbations along the  $y$  direction, i.e., transverse perturbations. To attack this nontrivial nonlinear problem from an analytical perspective, we utilize the average Lagrangian formalism [39] to reduce the dimensionality of the system. The idea is to assume the modulation of a bion stripe by allowing its parameters,  $v$ ,  $\phi$ , and  $\tau$  to be functions of  $y$  and  $t$ . This treats the bion stripe as a soliton filament or bendable, tubelike curve whose local cross section is the bion solution (9) that can expand and contract as dictated by the corresponding Lagrangian (and the resulting Euler-Lagrange equations). We remark that another, similar approach to studying the transverse dynamics of soliton filaments in other areas of nonlinear physics utilizes an effective Hamiltonian [42]. By substituting the bion stripe solution (9) into the Lagrangian (7) and integrating over  $x$ , we obtain the averaged Lagrangian. For simplicity of presentation, we restrict to the low frequency and small velocity regime where bion stripes approach static stripe domains and can be topologically classified by the sign of the precessional frequency. The more general case can be studied in the same manner but the expressions become more complicated. In the  $|\phi| \ll |\dot{\phi}| \ll 1$  case, asymptotic expansion in frequency, velocity, space, and time give the leading-order averaged Lagrangian (see Appendix for details)

$$L_{\text{avg}} = 2 \int \dot{\phi}^2 \gamma (V^2 + \dot{\phi}^2) \dot{\phi}^2 (\tau) \ln(V^2 + \dot{\phi}^2) + \dot{\phi}^2 \frac{\gamma(V^2 + \dot{\phi}^2)}{2(V^2 + \dot{\phi}^2)} + 4(\tau) \tan^{-1} \frac{\dot{\phi}^2 + \sqrt{V^2 + \dot{\phi}^2}}{V}, \tag{12}$$

where the capitalized variables  $\dot{\phi} = \dot{\phi}/|\phi|$ ,  $V = v/|\phi|$ ,  $T = |\phi|t$ , and  $Y = |\phi|y$  denote, respectively, the order one scaled frequency, velocity, time, and space variables by the small characteristic precessional frequency  $\phi$  of an unperturbed bion stripe.

The averaged equations of motion are the Euler-Lagrange equations of the averaged Lagrangian (12) (which can be expressed in a symmetric form

$$\tau \dot{\phi}^2 \frac{1}{2} \gamma \dot{\phi}^2 \dot{\phi}^2 e^u \cos u = 0, \tag{13a}$$

$$\tau \dot{\phi}^2 \frac{1}{2} \gamma \dot{\phi}^2 u \dot{\phi}^2 e^u \sin u = 0, \tag{13b}$$

$$\tau + 2 \gamma \dot{\phi}^2 = 0, \tag{13c}$$

$$\tau u + 2 \gamma \dot{\phi}^2 = 0, \tag{13d}$$

with the change of variables

$$V = \frac{v}{|\phi|}, \quad \dot{\phi} = \frac{\dot{\phi}}{|\phi|}, \quad \tau = |\phi|t, \quad u = \phi y$$

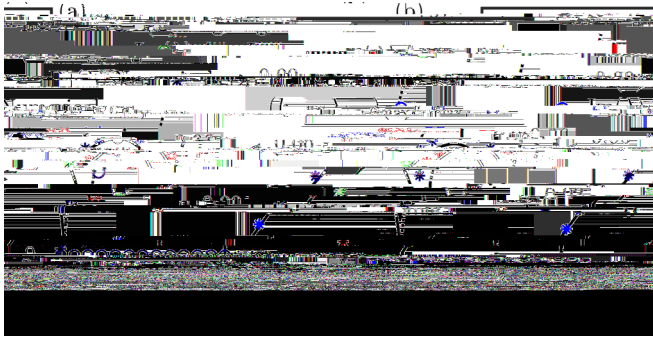


FIG. 2. Growth rates for the (a) nontopological  $\omega_0 = 0.06$  and (b) topological  $\omega_0 = \pi - 0.06$  bion stripes. The maximally unstable wavelength and maximal growth rate  $k_{\max}$  and  $\gamma_{\max}$  are indicated by a red black circle in (a). Numerical calculations are shown by blue asterisks and circles for the real and imaginary growth rates, respectively.

in the nature of the instability of nontopological and topological bion stripes.

Our focus in this work is on stationary bion stripes for which  $V_0 = 0$ . In this case, the growth rate  $\gamma(k)$  becomes

$$\gamma(k) = K \sqrt{\tilde{\gamma} k^2 + 2} \quad (20)$$

because  $\omega_0 = \pm 1$ . All perturbations with wave number  $k$  in the unstable band  $(k_c, K_c)$ ,  $K_c = \sqrt{2}$ , lead to a transverse instability. The growth rate  $\gamma(k)$  is maximized for the wave number  $k_{\max} = 1$  and attains the maximal growth rate  $\gamma_{\max} = 1$ . Returning to the lowercase unscaled wave number  $k$  and growth rate  $\gamma$ , the maximally unstable wave number, maximal growth rate, and unstable wave-number band for an initial, stationary bion stripe with frequency  $\omega_0$  are

$$k_{\max} = \frac{1}{|\omega_0|}, \quad \gamma_{\max} = |\omega_0|, \quad k_c = \frac{\sqrt{2}}{|\omega_0|}. \quad (21)$$

The dominant growth rate, wavelength of instability, and unstable band are the same for topological ( $\omega_0 < 0$ ) and nontopological ( $\omega_0 > 0$ ) bion stripes.

We have also performed a linearization of the Larmor torque equations (3) and (4) about the bion stripe solution (9). This leads to a linear eigenvalue problem for small perturbations of the magnetization vector. Direct numerical computation yields a definitive prediction for the unstable mode and its growth rate dependence on the transverse wave number. The details are described in Appendix B. To remove phase singularities, we must consider small but nonzero  $\epsilon$  for topological bions (

vector at the maximal growth rate  $\gamma_{\max} = 1$  and associated wave number  $k_{\max} = 1$  while assuming an initial perturbation of small amplitude  $a$  in this unstable direction, we find that the bion phase and frequency exhibit exponential temporal growth

$$\begin{aligned} \phi(Y,T) &= T + \frac{a}{5} e^T \cos Y, & \omega(Y,T) &= 1 + \frac{2a}{5} e^T \cos Y, \end{aligned} \tag{23}$$

whereas the bion center  $\phi(Y,T) = 0$  and velocity  $\omega(Y,T) = 0$  do not. This implies that the nontopological bion exhibits a transverse instability whose initial development is dominated by fluctuations in the bion's phase and frequency. Because the bion width  $W$  [recall Eq. (1)] depends on the local bion frequency, we expect to see the development of fluctuations in  $\phi(Y,T)$  during the initial stage of the transverse instability with negligible variation in the soliton filament's center  $\omega(Y,T)$ . This is known as a neck transverse instability [4].

We also investigate the nature of the transverse instability in the topological case  $\phi_0 = \frac{1}{2}$  by dividing the eigenvector (19) by 2 and setting  $\gamma_0 = 0$  to obtain

$$\phi_0 = \frac{1}{2} \mathbf{1}: \quad \begin{pmatrix} 1 \\ 1 \\ 1 \\ u_1 \end{pmatrix} = \begin{pmatrix} 0 \\ 2K^2 \\ K \\ 0 \end{pmatrix}. \tag{24}$$

If we perturb in the most unstable direction (24), this time the exponential growth occurs in the bion center and velocity

$$\begin{aligned} \phi(Y,T) &= \frac{a}{5} e^T \cos Y, & \omega(Y,T) &= \frac{2a}{5} e^T \cos Y, \end{aligned} \tag{25}$$

while the phase and frequency are stationary  $\phi(Y,T) = \frac{1}{2}$ ,  $\omega(Y,T) = \frac{1}{2}$  for a perturbation amplitude  $a = 1$ . The growth of variation in the topological bion's center is called a snake instability; see, e.g., Ref. [5] for a recent discussion.

From the numerical calculations, we have also obtained the spatial eigenfunctions for the unstable modes. The eigenfunctions are indicated with the subscript 1 and represent deviations from the uniform bion stripe. Figure 5 shows the maximally unstable mode in the non-topological [Fig. 5(a)] and topological [Fig. 5(b)] cases. The structure of the unstable mode coincides with the predictions from the average Lagrangian theory. In particular, the  $u_{1,z}$  and  $u_1$  modes are in phase. The nontopological case exhibits a symmetric mode that, when added to the bion, leads to a periodic reduction and increase in the bion's width, manifesting a precursor of the neck instability. In the topological case, the mode is antisymmetric and, when added to the bion, leads to a periodic shift from left to right of the bion's center, suggesting the onset of the snake instability. We were unable to perform a direct linearization of the topological bion stripe because of its phase jump at  $x = \phi(t)$ . Instead, we linearized nontopological, propagating

FIG. 6. Evolution of the width  $w$  of an initially perturbed, nontopological bion stripe with  $\omega_0 = 0.06$ . Direct numerical simulations of the Larmor torque equation (solid) and the average Lagrangian equations (dashed) show excellent agreement. The time scale for the average Lagrangian results have been scaled by the ratio  $\omega_{\max}/\omega_0 = 1.06$  where  $\omega_0$  is the maximum growth rate from numerical linearization.

the nontopological averaged Lagrangian numerics, with the frequency perturbation scaled by  $\omega_0$ . The width is extracted from Larmor simulations by interpolating the numerical solution to find  $x_{\pm}(y, t) < x_{\pm}(y, t)$  such that  $m_z(x_{\pm}, y, t) = 0$ . The width reported in Fig 6 (solid curves) is  $w = x_+ - x_-$ . The average Lagrangian equations are in excellent agreement with the full Larmor torque equation, even well beyond the linear regime.

In Fig. 6, we observe significant amplitude growth and deviation from a sinusoidal waveform to one in which the soliton width approaches zero, the neck instability. Zero width corresponds to pinching of the soliton filament and the breakdown of the single soliton filament approximation. The soliton filament center remains at zero throughout the simulation. Longer evolution leads to a significant increase in the frequency  $\omega$ , beyond the regime of validity,  $\omega = O(1)$ , and therefore signals the breakdown of the average Lagrangian approach. We will investigate the pinching of the soliton filament and subsequent evolution in Sec. 4.

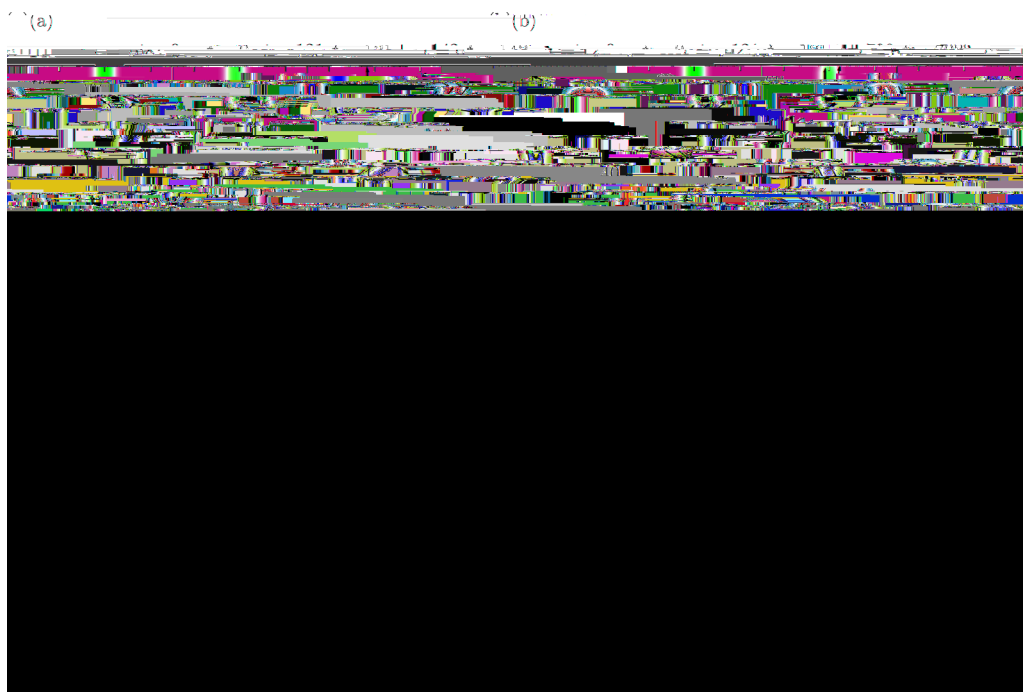
We now investigate the nonlinear stage of evolution of the topological bion filament. Figures 7(a) and 7(b) display the evolution of the soliton filament width  $w$  and center  $x_c$ , respectively, from numerics of both the average Lagrangian equations (dashed line) and the Larmor torque equation (solid line). Again, we rescale time in these figures by  $\omega_{\max}/\omega_0$  according to the small difference in the maximal growth rates. Here, the average Lagrangian equations (3) are initialized with a stationary topological bion perturbed in the maximally unstable direction (24) with amplitude  $a = 10^{-3}$ . The Larmor torque equation is initialized with a bion stripe with frequency  $\omega_0 = 0.06$  and the same sinusoidal perturbation, now with the  $v$  component scaled by  $|y_0|$ . The initially small soliton filament center modulation grows rapidly with wave number  $k_{\max}$ , as predicted by linear stability analysis in Eq. (25). Recall that the soliton filament width is predicted to not exhibit growth during the linear stage of evolution. This is consistent with Fig. 7(b) where an initially constant width takes some time to develop even small amplitude oscillations. Moreover, these oscillations exhibit the wave number  $k_{\max}/2$ , the second harmonic of the maximally unstable mode, and is due to the nonlinear coupling of the soliton filament parameters in

FIG. 7. Numerical evolution of a perturbed, topological bion stripe with  $\omega_0 = 0.06$  according to the average Lagrangian equations (dashed) and the Larmor torque equation (solid). (a) The soliton filament width  $w$ . (b) The soliton filament center  $x_c$ . For both, the time scale for the average Lagrangian results have been scaled by the ratio  $\omega_{\max}/\omega_0 = 1.11$  where  $\omega_0$  is the maximum growth rate from numerical linearization.

Eqs. (13). As in the case of the nontopological bion filament, the topological bion filament also exhibits breakup into two-dimensional coherent structures, signaling the breakdown of the average Lagrangian theory. We now investigate this regime.

### V. BREAKUP OF A BION FILAMENT

In this section, we perform time-dependent numerical simulations for a bion stripe subject to small transverse perturbations. We discretize Eqs (3) and (4) with no applied field. Utilizing a periodic boundary, pseudospectral method in space [46], we integrate in time with a fourth-order Runge-Kutta method. The domain is discretized into a mesh of  $1286 \times 1286$  grid points with  $0.5$





breakup. We base this observation on work in Ref. [26] that numerically demonstrated how two adjacent, in-phase droplets attract and form a long-lived breather solution that resembles what we observe here. For the topological bion, we can predict how topological poles form within the bion filament. The limit  $v \rightarrow 0^\pm$  in the phase yields a phase jump for  $\alpha < 0$ , as noted in Eq. (10). For small but nonzero  $v$ , we have the expansion of Eq. (9b):

$$\phi(x,y,t) \approx \frac{v(x, \tilde{S})}{2} + \tan^{-1} \frac{F(\tilde{S}) \tanh(\tilde{S}^{-1} [x - \tilde{S}t])}{v}, \quad (27)$$

where  $F(\tilde{S}) = 2|v|/\tilde{S} > 0$ . Equation (27) expresses the smoothing of the phase jump by a nonzero velocity. The phase jump is negative when  $v < 1$  and positive for  $0 < \tilde{S}v < 1$ . Therefore, when the velocity  $v(Y, T)$  passes through zero with  $v_Y < 0$  or  $v_Y > 0$ , a topological pole is formed. The sign of the pole's skyrmion number  $S$  [recall Eq. (2)] is opposite the spatial slope  $\alpha$ , i.e.,  $\text{sgn} S = -\tilde{S} \text{sgn} v_Y$ . Because there are two velocity zero crossings per period of the instability, we can write the poles per unit length as

$$N_p = \frac{|\alpha|}{2} \quad (28)$$

which, for  $L_y = 128$ ,  $N_p L_y = 10$  agrees with the simulation in Fig. 8(b). Note that this is simply twice Eq. (26).

### VI. DISCUSSION: MAGNETICALLY DAMPED BION STRIPES

So far, the analysis presented here has neglected the role of damping. Because magnetic damping drives the magnetization to a static configuration, it is an additional source of instability for a bion stripe. While one might expect damping to play a



by many terms in  $\mathbf{L}$ . While this integration is not theoretically difficult, the Lagrangian that is obtained from the process linearized equation for  $\mathbf{m}_1$  is found to be turns out to be complicated unless additional assumptions are made on the bion's frequency and velocity  $v$ . The obtained average Lagrangian is therefore asymptotically expanded assuming  $|\hat{\mathbf{y}}| \ll |v| \ll 1$ . The result, in scaled variables, is given in Eq. (12).

$$\begin{aligned} \mathbf{m}_1(\hat{\mathbf{y}}, t) = v \mathbf{m}_1 + & (m_{1,y} \hat{x} \hat{S} m_{1,x} \hat{y}) \\ & \hat{S} m_0 \times (\hat{y}^2 m_1 + m_{1,z} \hat{z}) \\ & \hat{S} m_1 \times (\hat{y}, m_0 + m_{0,z} \hat{z}). \end{aligned} \quad (B2)$$

APPENDIX B: LINEARIZED LARMOR TORQUE EQUATION ABOUT THE BION STRIPE

Starting with the Larmor torque equations (3) and (4), we linearize about the bion stripe solution. We assume that the magnetization can be written  $\mathbf{m} = \mathbf{m}_0 + \mathbf{m}_1$ , where  $\mathbf{m}_0$  is obtained by substituting the bion stripe solution in Eqs. (8) and (9b) into Eq. (5). We are interested in linearizing about the stationary bion stripe, however, the topological bion exhibits a discontinuity at  $x = 0$ . Therefore, for numerical stability purposes, we will consider the parameter regime  $|\hat{\mathbf{y}}| \ll 1$  for the topological bion, which smooths the discontinuity at  $x = 0$  without drastically changing the dispersion relation. For the nontopological bion, we are free to assume  $v = 0$ .

Because we are interested in bion stripes with a finite velocity  $v$ , we transform coordinates to a moving reference frame  $\hat{\mathbf{x}} = \hat{\mathbf{x}} \hat{S} v t$ . We can remove the explicit time dependence by applying a rotation matrix

$$R(\hat{\mathbf{y}}) = \begin{pmatrix} \cos(\hat{\mathbf{y}}) & \hat{S} \sin(\hat{\mathbf{y}}) & 0 \\ \sin(\hat{\mathbf{y}}) & \cos(\hat{\mathbf{y}}) & 0 \\ 0 & 0 & 1 \end{pmatrix} \quad (B1)$$

By construction  $\mathbf{m}_0$  is only a function of  $\hat{\mathbf{y}}$ , so we may assume a linear wave solution  $\mathbf{m}_1$  and:

$$\mathbf{m}_1(\hat{\mathbf{y}}, t) = \tilde{\mathbf{m}}_1(\hat{\mathbf{y}}) e^{i(k_y \hat{S} \mu t)}. \quad (B3)$$

The substitution of Eq. (B3) into (B2) yields the eigenvalue problem

$$\mu \mathbf{B3}$$

- [19] S. Lendínez, N. Statuto, D. Backes, A. D. Kent, and F. Macià, Observation of droplet soliton drift resonances in a spin-transfer-torque nanocontact to a ferromagnetic thin film, *Phys. Rev. B* **92**, 174426 (2015).
- [20] S. Chung, A. Eklund, E. Iacocca, S. M. Mohseni, S. R. Sani, L. Bookman, M. A. Hofer, R. K. Dumas, and J. Kerman, Magnetic droplet nucleation boundary in orthogonal spin-torque nano-oscillators, *Nat. Commun* **7**, 11209 (2016).
- [21] S. Mühlbauer, B. Binz, F. Jonietz, C. Pfleiderer, A. Rosch, A. Neubauer, R. Georgii, and P. Böni, Skyrmion lattice in a chiral magnet, *Science* **323**, 915 (2009).
- [22] X. Z. Yu, Y. Onose, N. Kanazawa, J. H. Park, J. H. Han, Y. Matsui, N. Nagaosa, and Y. Tokura, Real-space observation of a two-dimensional skyrmion crystal, *Nature (London)* **465**, 901 (2010).
- [23] W. Jiang, P. Upadhyaya, W. Zhang, G. Yu, M. B. Jung, F. Y. Fradin, J. E. Pearson, Y. Tserkovnyak, K. L. Wang, O. Heinonen et al., Blowing magnetic skyrmion bubbles, *Science* **349**, 283 (2015).
- [24] W. Jiang, X. Zhang, G. Yu, W. Zhang, X. Wang, M. B. Jung, J. E. Pearson, X. Cheng, O. Heinonen, K. L. Wang et al., Direct observation of the skyrmion hall effect, *Nat. Phys.* **13**, 162 (2017).
- [25] S. A. Montoya, S. Couture, J. J. Chess, J. C. T. Lee, N. Kent, D. Henze, S. K. Sinha, M.-Y. Im, S. D. Kevan, P. Fischer et al., Tailoring magnetic energies to form dipole skyrmions and skyrmion lattices, *Phys. Rev. B* **95**, 024415 (2017).
- [26] Y. Zhou, E. Iacocca, A. Awad, R. K. Dumas, H. B. Zhang, H. B. Braun, and J. Kerman, Dynamically stabilized magnetic skyrmions, *Nat. Commun* **6**, 8193 (2015).
- [27] A. Fert, V. Cros, and J. Sampaio, Skyrmions on the track, *Nat. Nanotechnol.* **8**, 152 (2013).
- [28] X. Zhang, M. Ezawa, and Y. Zhou, Magnetic skyrmion logic gates: Conversion, duplication and merging of skyrmions, *Sci. Rep.* **5**, 9400 (2015).
- [29] M. D. Maiden, L. D. Bookman, and M. A. Hofer, Attraction, merger, refection, and annihilation in magnetic droplet soliton scattering, *Phys. Rev. B* **89**, 180409 (2014).
- [30] S.-Z. Lin, C. D. Batista, and A. Saxena, Internal modes of a skyrmion in the ferromagnetic state of chiral magnets, *Phys. Rev. B* **89**, 024415 (2014).
- [31] D. Xiao, V. Tiberkevich, Y. H. Liu, Y. W. Liu, S. M. Mohseni, S. Chung, M. Ahlberg, A. N. Slavin, J. Kerman, and Y. Zhou, Parametric autoexcitation of magnetic droplet soliton perimeter modes, *Phys. Rev. B* **95**, 024106 (2017).
- [32] J.-Y. Lee, K.-S. Lee, S. Choi, K. Y. Guslienko, and S.-K. Kim, Dynamic transformations of the internal structure of a moving domain wall in magnetic nanostripes, *Phys. Rev. B* **76**, 184408 (2007).
- [33] Y. Yoshimura, K.-J. Kim, T. Taniguchi, T. Tono, K. Ueda, R. Hiramatsu, T. Moriyama, K. Yamada, Y. Nakatani, and T. Ono, Soliton-like magnetic domain wall motion induced by the interfacial Dzyaloshinskii-Moriya interaction, *Nat. Phys.* **12**, 157 (2015).
- [34] E. Iacocca, R. K. Dumas, L. Bookman, M. Mohseni, S. Chung, M. A. Hofer, and J. Kerman, Con ned Dissipative Droplet Solitons in Spin-Valve Nanowires with Perpendicular Magnetic Anisotropy, *Phys. Rev. Lett* **112**, 047201 (2014).
- [35] O. Heinonen, W. Jiang, H. Somaily, S. G. E. te Velthuis, and A. Hoffmann, Generation of magnetic skyrmion bubbles by inhomogeneous spin hall current, *Phys. Rev. B* **93**, 094407 (2016).
- [36] S.-Z. Lin, Edge instability in a chiral stripe domain under an electric current and skyrmion generation, *Phys. Rev. B* **94**, 020402 (2016).
- [37] Y. Liu, N. Lei, W. Zhao, W. Liu, A. Ruotolo, H.-B. Braun, and Y. Zhou, Chopping skyrmions from magnetic chiral domains with uniaxial stress in magnetic nanowires, *Appl. Phys. Lett* **111**, 022406 (2017).
- [38] M. Ma, R. Carretero-González, P. G. Kevrekidis, D. J. Frantzeskakis, and B. A. Malomed, Controlling the transverse instability of dark solitons and nucleation of vortices by a potential barrier, *Phys. Rev. A* **82**, 023621 (2010).
- [39] B. A. Malomed, in *Progress in Optics* (Elsevier, Amsterdam, 2002), pp. 69–191.
- [40] G. Chen, J. Zhu, A. Quesada, J. Li, A. T. N'Diaye, Y. Huo, T. P. Ma, Y. Chen, H. Y. Kwon, C. Won, Z. Q. Qiu, A. K. Schmid, and Y. Z. Wu, Novel Chiral Magnetic Domain Wall Structure in Fe/Ni/Cu(001) Films, *Phys. Rev. Lett* **110**, 177204 (2013).
- [41] S. Emori, U. Bauer, S.-M. Ahn, E. Martinez, and S. D. Beach, Current-driven dynamics of chiral ferromagnetic domain walls, *Nat. Mater.* **12**, 611 (2013).
- [42] P. G. Kevrekidis, W. Wang, R. Carretero-Gonzalez, and D. J. Frantzeskakis, Adiabatic Invariant Approach to Transverse Instability: Landau Dynamics of Soliton Filaments, *Phys. Rev. Lett.* **118**, 244101 (2017).
- [43] V. A. Mironov, A. I. Smirnov, and L. A. Smirnov, Dynamics of vortex structure formation during the evolution of modulation instability of dark solitons, *JETP* **112**, 46 (2011).
- [44] D. V. Skryabin and W. J. Firth, Modulational Instability of Solitary Waves in Nondegenerate Three-Wave Mixing: The Role of Phase Symmetries, *Phys. Rev. Lett* **81**, 3379 (1998).
- [45] M. A. Hofer and B. Ilan, Onset of transverse instabilities of con ned dark solitons, *Phys. Rev. A* **94**, 013609 (2016).
- [46] M. A. Hofer and M. Sommacal, Propagating two-dimensional magnetic droplets, *Phys. D (Amsterdam)* **241**, 890 (2012).
- [47] Y. S. Kivshar and B. A. Malomed, Dynamics of solitons in nearly integrable systems, *Rev. Mod. Phys.* **61**, 763 (1989).
- [48] L. D. Bookman and M. A. Hofer, Perturbation theory for propagating magnetic droplet solitons, *Proc. R. Soc. London A* **471**, 20150042 (2015).
- [49] P. G. Kevrekidis, G. Theocharis, D. J. Frantzeskakis, and A. Trombettoni, Avoiding infrared catastrophes in trapped bose-einstein condensates, *Phys. Rev. A* **70**, 023602 (2004).
- [50] I. E. Dzyaloshinskii, A thermodynamic theory of weak ferromagnetism of antiferromagnetics, *Phys. Chem. Solids* **4**, 241 (1958).
- [51] T. Moriya, Anisotropic superexchange interaction and weak ferromagnetism, *Phys. Rev.* **120**, 91 (1960).